THE JOURNAL OF BIOLOGICAL CHEMISTRY VOL. 289, NO. 40, pp. 27911–27923, October 3, 2014
© 2014 by The American Society for Biochemistry and Molecular Biology, Inc. Published in the U.S.A.

Electrostatic Interactions in the Binding Pathway of a Transient Protein Complex Studied by NMR and Isothermal Titration Calorimetry*

Received for publication, July 9, 2014, and in revised form, August 8, 2014 Published, JBC Papers in Press, August 13, 2014, DOI 10.1074/jbc.M114.553354

Erick Meneses and Anthony Mittermaier[1]

From the Department of Chemistry, McGill University, Montreal, Québec H3A 0B8, Canada

Background: Electrostatic interactions are known accelerate binding in protein complexes with long lifetimes (minutes to hours).
Results: NMR and calorimetry were used to characterize binding kinetics in short lived (~1 ms) protein-peptide complexes.
Conclusion: Electrostatic enhancement is much less and basal (electrostatic-free) association rates are greater than previously observed.
Significance: Electrostatics may play different roles in short lived and long lived protein complexes.

Much of our knowledge of protein binding pathways is derived from extremely stable complexes that interact very tightly, with lifetimes of hours to days. Much less is known about weaker interactions and transient complexes because these are challenging to characterize experimentally. Nevertheless, these types of interactions are ubiquitous in living systems. The combination of NMR relaxation dispersion Carr–Purcell–Meiboom–Gill (CPMG) experiments and isothermal titration calorimetry allows the quantification of rapid binding kinetics for complexes with submillisecond lifetimes that are difficult to study using conventional techniques. We have used this approach to investigate the binding pathway of the Src homology 3 (SH3) domain from the Fyn tyrosine kinase, which forms complexes with peptide targets whose lifetimes are on the order of about a millisecond. Long range electrostatic interactions have been shown to play a critical role in the binding pathways of tightly binding complexes. The role of electrostatics in the binding pathways of transient complexes is less well understood. Similarly to previously studied tight complexes, we find that SH3 domain association rates are enhanced by long range electrostatics, whereas short range interactions are formed late in the docking process. However, the extent of electrostatic association rate enhancement is several orders of magnitudes less, whereas the electrostatic-free basal association rate is significantly greater. Thus, the SH3 domain is far less reliant on electrostatic enhancement to achieve rapid association kinetics than are previously studied systems. This suggests that there may be overall differences in the role played by electrostatics in the binding pathways of extremely stable *versus* transient complexes.

Many biological processes rely on the rapid formation of protein-ligand complexes (1–5). Consequently, there has been great interest in elucidating the mechanisms through which binding partners are able to efficiently recognize each other in solution and adopt the correct conformations, relative positions, and orientations to form native stereo-specific complexes. This has been addressed theoretically (6, 7), by computer simulation (8, 9), and experimentally (1, 5, 10, 11). The association process is typically broken down into at least two steps. In the first step, the binding partners encounter each other through a random collision. For the small fraction of collisions in which the binding surfaces are correctly aligned (as few as 1 in 10^5), the molecules proceed to the second step and dock to form the native stereo-specific complex (12). If the docking step occurs much more rapidly than the time scale of productive intermolecular collisions, the reaction is said to be "diffusion-controlled," and the association rate is viscosity-dependent (6). When binding is diffusion-controlled, the protein and ligand pass through a free energy maximum en route to the bound state, in which translational-rotational entropy is reduced with little compensation from favorable interactions (12, 13). The ensemble of conformations at this free energy maximum has been referred to as an "encounter complex" (6), "transient complex" (14), or "transition state" (15). We shall use the term "transition state" throughout. For these systems, binding is essentially two-state, such that significant populations are observed only for the free and/or bound states, and a negligible fraction of molecules populate the high-energy transition state at any one time. Note that the two-state diffusion-controlled binding mechanism is compatible with conformational changes occurring after the transition state, provided that they proceed sufficiently rapidly (16). Additionally, transient conformational reorganization can occur prior to the intermolecular collision, leading to a "gated" diffusion-controlled binding mechanism (17). In either case, the structure of the transition state is key to understanding the binding pathway because it represents a kinetic bottleneck. Interactions that stabilize the transition state accelerate molecular association rates (6, 14, 15).

* This work was supported by a grant from the Natural Sciences and Engineering Research Council (NSERC) of Canada.
[1] A member of Groupe de Recherche Axé sur la Structure des Protéines (GRASP). To whom correspondence should be addressed: Dept. of Chemistry, McGill University, 801 Sherbrooke St. W., Rm. 322, Montreal, Québec H3A 0B8, Canada. Tel.: 514-398-3085; Fax: 514-398-3797; E-mail: anthony.mittermaier@mcgill.ca.

TABLE 1
Electrostatic enhancement of protein association rates

	MW (Da)	Net charge	K_A (M^{-1})	k_{off} (s^{-1})	Basal k_{on} M^{-1} S^{-1}	Enhancement
Fyn SH3 domain	6979	-8				
RR peptide	1444	+2	51.7×10^{5} [a]	235 [a]	6.57×10^{7}	23.1
SR peptide	1375	+1	6.31×10^{5} [a]	378 [a]	5.94×10^{7}	4.42
SS peptide	1306	0	2.71×10^{3} [a]	1829 [a]	5.71×10^{7}	-
Barnase (26)	12382	+2				
Barstar	10342	-6	7.5×10^{13} [b]	8×10^{-6} [b]	3.98×10^{6}	1.92×10^{3}
Shaker K+ channel (66)	74193	-13				
Peptide toxin Lq2	4360	+5	3.0×10^{9} [b]	0.19 [b]	3.66×10^{5}	6.40×10^{4}
E9 DNase (67)	61587	+4				
Immunity protein Im9	9582	-9	1.4×10^{16} [b]	0.41×10^{-6} [b]	1.25×10^{6}	4.50×10^{5}
Heterodimeric leucine zipper (68)						
Acidic chain	1864	-4	1.9×10^{11} [c]	0.38×10^{-3} [c]	5.88×10^{5}	4.50×10^{3}
Basic chain	3402	+9				
Acetylcholinesterase (1)	68168	-9				
Fasciculin	6757	+4	1.3×10^{13} [b]	1.0×10^{-4} [b]	1.97×10^{5}	8.81×10^{3}

[a] Measurement obtained at $I = 2$ mM.
[b] Measurement obtained at $I = 25$ mM.
[c] Measurement obtained at $I = 74$ mM.

A variety of interactions have been proposed to contribute to the stability of transition states, including nonspecific hydrogen bonding, van der Waals interactions, non-polar desolvation, long range electrostatic interactions (6, 18–20), or subsets of native bound-like interactions (21). The role of electrostatics in binding pathways has been particularly well studied. For a number of systems, including barnase-barstar (5), E9-Im9 (10), IL4-IL4BP (11), and Fas-AchE (1), it has been found that electrostatic stabilization of weakly specific transition states can accelerate association by up to 4 or more orders of magnitude, compared with the basal rate (15). A combination of experimental and computational studies has led to a picture of the transition state in which the binding partners remain solvent-separated and interact almost exclusively by long range electrostatics (15, 22).

However, these investigations have focused on extremely tight protein-ligand interactions, as listed in Table 1. Equilibrium association constants have ranged from 10^{9} to 10^{13} M^{-1} (K_D nanomolar to picomolar), with dissociation rates of 10^{-1} to 10^{-6} s^{-1} (lifetimes of seconds to days) Much less is known about the binding pathways of weaker complexes with lifetimes on the order of milliseconds. These types of short lived protein interactions are abundant in nature, raising the important question of to what extent long lived and short lived complexes follow similar binding pathways. In what follows, we will use "long lived" to refer to complexes that bind with $<$nM K_D and have lifetimes on the order of minutes or longer. We will use "short lived" to refer to complexes with at least micromolar K_D and lifetimes on the order of milliseconds. Several studies of short lived complexes have derived structural models of transient complexes that precede formation of the fully bound state (23–25). However, these investigations did not extract kinetic parameters or identify the interactions governing association rates, which is key to understanding binding pathways.

The binding kinetics of short lived complexes are challenging to measure experimentally. In typical stopped-flow binding measurements, the protein and ligand are rapidly mixed, and the extent of the reaction is monitored as a function of time using techniques including spectroscopic absorbance (21), fluorescence (10, 26, 27), enzymatic activity (1, 28, 29), and surface plasmon resonance (30, 31). These techniques are limited by the requirement that the lifetimes of the free and bound states must be severalfold longer than the time required to completely mix the protein and ligand solutions; otherwise, the reaction proceeds nearly to completion before the start of the measurement period.

The combination of nuclear magnetic resonance (NMR) spectroscopy and isothermal titration calorimetry (32) can characterize binding kinetics that are too rapid for standard stopped-flow techniques, on the order of 10^{4} s^{-1} (33). In this approach, a substoichiometric amount of ligand is added to a protein sample whose signals are monitored by NMR spectros-

copy. The resulting dynamical exchange between the free and bound states modulates the chemical shifts of nuclei in the protein on the millisecond to microsecond time scale, leading to signal broadening. The broadening is quantified by NMR relaxation dispersion experiments (34–36), which yield the dissociation rate constant, k_{off}. The equilibrium association constant of the interaction, K_a, is determined by ITC or NMR titration experiments. The second-order association rate constant is then given by the equation, $k_{on} = K_a \cdot k_{off}$. These two parameters report on the binding pathway because K_a is related to the free energy difference between the free and bound states, whereas k_{on} is related to the free energy difference between the free state and the transition state.

Src homology 3 (SH3)[2] domains are typical of weakly binding proteins that form short lived complexes. These ~60-amino acid modules are found in the context of larger multidomain proteins and mediate protein-protein interactions in signal transduction pathways (37, 38). The type I ligand recognized by many SH3 domains comprises a short peptide sequence, $+X\Phi PX\Phi P$, where P is proline, Φ is a hydrophobic amino acid, X is any amino acid, and + is a positively charged residue, typically arginine or lysine (38). The positions in the motif are numbered −3 to 3 such that the conserved + occupies site −3. Dissociation constants for SH3 domains are usually on the order of micromolar, and the lifetimes of their complexes are on the order of milliseconds (33, 39). We previously used NMR and ITC to study the binding kinetics of the SH3 domain from the Fyn tyrosine kinase. We showed that this protein binds a type I target peptide in a two-state manner with millisecond time scale kinetics and a temperature dependence of k_{on} that is consistent with diffusion-limited association (33). In the current study, we have focused on how positively charged residues within the SH3 binding motif and negatively charged residues in the binding site on the SH3 domain interact to influence association kinetics. Three different dodecapeptides were employed: one with a typical type I consensus motif with the conserved Arg^{-3} preceded by Ser^{-4} (SR, net charge +1), a second containing $R^{-4}R^{-3}$ (RR, net charge +2), and a third containing $S^{-4}S^{-3}$ (SS, net charge 0). We analyzed the contributions of the conserved Arg^{-3} and "extra" Arg^{-4} residues to the stabilities of the fully bound and transition states by comparing the binding affinities and association rates of the RR, SR, and SS peptides. Data were extrapolated to both zero ionic strength, where long range electrostatic interactions are maximal, and infinite ionic strength, where long range electrostatics are fully attenuated. We find that the conserved Arg^{-3} and the "extra" Arg^{-4} residues stabilize both the encounter and fully bound complexes via similar long range electrostatic interactions, which implies that the Fyn SH3 domain and peptide are fairly close in the transition state. Notably, Arg^{-3} additionally stabilizes the bound state via short range interactions that are not screened by adding salt. Likely candidates include a network of salt bridges and hydrogen bonds previously observed for this residue in the bound complex by NMR (40) and x-ray crystallography (Protein Data Bank entry 4EIK). These short range interactions involving Arg^{-3} are not present in the transition state and are only made after the molecules have crossed the free energy barrier, near the end of the binding pathway. Thus, the SH3-peptide transition state is fairly compact and stabilized primarily by long range electrostatic interactions, as seen for other protein-ligand systems (5, 14, 15, 22). However, there are surprising differences between the system studied here and the high-affinity long lived complexes investigated previously. We find that the electrostatic-free basal association rate for this system is significantly greater, whereas the electrostatic association rate enhancement is several orders of magnitude less. This result suggests that short lived complexes may rely less on electrostatic enhancement to achieve rapid binding than do high-affinity long lived complexes.

[2] The abbreviations used are: SH3, Src homology 3; ITC, isothermal titration calorimetry; CPMG, Carr–Purcell–Meiboom–Gill; HSQC, heteronuclear single quantum coherence spectroscopy.

MATERIALS AND METHODS

Protein and Peptide Preparation—Wild-type chicken Fyn SH3 domain (residues 81–148) was expressed and purified as described previously (41). RR (Ac-WSLA$R^{-4}R^{-3}P^{-2}L^{-1}P^0P^1L^2P^3$-$NH_2$), SR (Ac-WSLA$S^{-4}R^{-3}P^{-2}L^{-1}P^0P^1L^2P^3$-$NH_2$), and SS (Ac-WSLA$S^{-4}S^{-3}P^{-2}L^{-1}P^0P^1L^2P^3$-$NH_2$) peptides were purchased from the Sheldon Biotechnology Centre (McGill University) and purified to homogeneity by reverse-phase HPLC. Protein and peptide samples were dialyzed against 5 mM MES, pH 6.0, at the desired NaCl concentration. For ionic strength calculations, it was assumed that the buffer contributed 2.57 mM charged ions. Most experiments were performed at 40 °C. This temperature was chosen to optimize the NMR CPMG relaxation dispersion profiles obtained with the RR and SR peptides and lies within the physiological temperature range of 40–42 °C (42).

ITC—Titrations were performed at 40 °C using a VP-ITC instrument (MicroCal LLC, Northampton, MA). Measurements were taken in triplicate for each NaCl concentration and consisted of 56 injections of 5 μl. RR peptide data were collected at 0.00, 0.01 0.03, 0.05, 0.10, 0.20, 0.30, 0.40, 0.50, 1.00, 1.50, and 2.00 M NaCl. For the SR and the SS peptide, measurements were taken at 0.00, 0.03, 0.20, and 0.30 M NaCl. Titrations were repeated for the SS peptide at 20 °C. Data were fitted using the one-set-of-independent-sites model in the Origin Software package (OriginLab, Northampton, MA) and in-house MATLAB scripts (MATLAB R2013a, The MathWorks, Natick, MA).

NMR—^1H-^{15}N HSQC titration spectra, referenced to an internal 4,4-dimethyl-4-silapentane-1-sulfonic acid standard (43), were collected at 40 °C and 800 MHz for samples containing ~0.3 mM protein and 16 different peptide concentrations. In the case of the SS peptide titration, chemical shift peak trajectories were fit globally according to Ref. 44,

$$\delta = \delta_{free} + \frac{1}{2}(\delta_{bound} - \delta_{free})(b - \sqrt{b^2 - 4R}) \qquad \text{(Eq. 1)}$$

where δ_{free} and δ_{bound} are the chemical shifts of the free and bound protein, $R = [peptide]_{total}/[protein]_{total}$, and $b = 1 + R + (K_a \times [protein]_{total})^{-1}$.

^1H-decoupled ^{15}N CPMG experiments (36) with power compensation schemes (33) were performed at 40 °C and 500 and

800 MHz on 1 mM samples of the Fyn SH3 domain, free in solution (0 M NaCl), in the presence of 0.1 mM SS, SR, and RR peptides (0, 0.2, 0.3 M NaCl) and with saturating amounts of the RR peptide (0 M NaCl). Measurements were repeated at 20 °C for the SH3 domain alone (0 M NaCl) and in the presence of 0.1 mM SS peptide (0, 0.2, and 0.3 M NaCl). Experiments employed a constant relaxation delay, T_{relax}, of 40 ms and 23 values of $\nu_{CPMG} = 1/(2\tau_{CP})$ ranging from 25 to 1000 Hz, where τ_{CP} is the delay between consecutive pulses. Transverse relaxation rates, R_2, were calculated for each cross-peak signal at each ν_{CPMG} value according to the following,

$$R_2^{exp}(\nu_{CPMG}) = -\frac{1}{T_{relax}}\ln\left(\frac{I(\nu_{CPMG})}{I_0}\right) \quad \text{(Eq. 2)}$$

where $I(\nu_{CPMG})$ is the peak intensity at a given value of ν_{CPMG}, and I_0 is the signal intensity with $T_{relax} = 0$. The experimental uncertainties in peak intensities (σ_I) were considered to be the same for all values of ν_{CPMG} for a given residue at a given ionic strength and static magnetic field. CPMG experiments were repeated for a subset of ν_{CPMG} values (N_{dup} different values), with n_j replicates obtained at the jth repeated ν_{CPMG} value. The n_j replicates obtained at $(\nu_{CPMG})_j$ for a given residue, ionic strength, and static magnetic field yield an S.D. value, s_j. The uncertainty in σ_I was calculated as follows,

$$\sigma_I^2 = \frac{\sum_{j=1}^{N_{dup}} s_j^2(n_j - 1)}{\sum_{j=1}^{N_{dup}} (n_j - 1)} \quad \text{(Eq. 3)}$$

and the associated errors in transverse relaxation rates, σ_{R2}, are given by the following.

$$\sigma_{R2}(\nu_{CPMG}) = \frac{\sigma_I I_0}{T_{relax} I(\nu_{CPMG})} \quad \text{(Eq. 4)}$$

CPMG data were fitted using a two-state model of conformational exchange,

$$P + L \underset{k_{off}}{\overset{k_{on}[L]}{\rightleftharpoons}} PL$$

REACTION 1

where P is the protein, L is the ligand, PL is the complex, k_{off} is the dissociation rate constant, k_{on} is the association rate constant, [L] is the concentration of free peptide, and the difference between the precession frequencies of an ^{15}N nucleus of the protein in the free and bound states is given by $\Delta\omega$. Dispersion profiles were fit to equations valid for the fast time scale regime (45) ($\Delta\omega \ll (k_{off} + k_{on}[L])$) or all time scale regimes (46) based on the parameter α,

$$\alpha = \frac{d\ln(R_{ex})}{d\ln(B_0)}, \quad \text{(Eq. 5)}$$

where R_{ex} is the total exchange contribution to R_2, and B_0 is the static magnetic field (47). Profiles with $\alpha > 1.5$ were considered to be in the fast exchange regime and were analyzed according to Ref. 45 as follows,

$$R_2(\nu_{CPMG}) = R_2^0 + \frac{\Phi_{ex}}{k_{ex}}\left(1 - \frac{4\nu_{CPMG}}{k_{ex}}\tanh\left(\frac{k_{ex}}{4\nu_{CPMG}}\right)\right) \quad \text{(Eq. 6)}$$

where p_{free} and p_{bound} are the relative populations of free and bound protein ($p_{free} + p_{bound} = 1$), $k_{ex} = k_{off} + k_{on}[L]$, $\Phi_{ex} = p_{free}p_{bound}\Delta\omega^2$, and $R_2{}^0$ is the population-weighted average (broadening-free) transverse relaxation rate ($R_2^0 = p_{free}R_{2free}^0 + p_{bound}R_{2bound}^0$). All other dispersion profiles were analyzed according to Ref. 46 as follows.

$$R_2(\nu_{CPMG}) = \frac{1}{2}(R_{2free}^0 + R_{2bound}^0 + k_{ex} - 2\nu_{CPMG}\cosh^{-1}(D_+\cosh(\eta_+) - D_-\cosh(\eta_-))) \quad \text{(Eq. 7)}$$

$$D_\pm = \frac{1}{2}\left(\pm 1 + \frac{\Psi + 2\Delta\omega^2}{\sqrt{\Psi^2 + \xi^2}}\right) \quad \text{(Eq. 8)}$$

$$\eta_\pm = \frac{\sqrt{2}}{4\nu_{CPMG}}\sqrt{\pm\Psi + \sqrt{\Psi^2 + \xi^2}} \quad \text{(Eq. 9)}$$

$$\Psi = (R_{2free}^0 - R_{2bound}^0 + p_{free}k_{ex} - p_{bound}k_{ex})^2 - \Delta\omega^2 + 4p_{free}p_{bound}k_{ex}^2 \quad \text{(Eq. 10)}$$

$$\xi = 2\Delta\omega(R_{2free}^0 - R_{2bound}^0 + p_{bound}k_{ex} - p_{free}k_{ex}) \quad \text{(Eq. 11)}$$

We performed the analysis assuming that $R_{2free}^0 = R_{2bound}^0$. This is typically done in analyses of CPMG data because it is not possible to reliably extract separate values for R_{2free}^0 and R_{2bound}^0 (48). In this case, the approximation is probably valid because binding of the peptide is unlikely to substantially alter ^{15}N transverse relaxation rates in the protein.

In the case of the RR and SR peptides at 40 °C with 0, 0.2, and 0.3 M NaCl, the data sets contained mixtures of dispersion profiles in the fast and intermediate time regimes, and data for all residues of a given sample were fitted simultaneously to extract global values of p_{bound} and k_{ex}, whereas $\Delta\omega^2$ or Φ_{ex}, R_2^0(800 MHz), and R_2^0(500 MHz) were obtained on a per-residue basis (49). For the SS peptide at 20 °C with 0 and 0.2 M NaCl, all but one of the dispersion profiles were in the fast time regime. In these cases, the value of p_{bound} was calculated based on the total concentrations of protein and peptide and the ITC-derived binding constants and was held fixed in the CPMG fits. Global values of k_{ex} were extracted, whereas $\Delta\omega^2$, R_2^0(800 MHz), and R_2^0(500 MHz) were obtained on a per-residue basis. Values of k_{off} were subsequently calculated as $(1 - p_{bound})k_{ex}$. Errors in the extracted parameters were estimated using a Monte Carlo approach in which group fitting was performed on random subsets of the residues selected using a bootstrap procedure (50). Analyses were performed using scripts written in MATLAB (MALAB R2011b, The MathWorks, Natick, MA).

Electrostatic Enhancements—$\mathrm{Log}_{10}(K_a)$ values for the SS peptide were fitted as a linear function of ionic strength. Interpolated values were used to calculate the affinity enhancements

of the SR and RR peptides. The corresponding linear interpolation was also used to calculate k_{on} enhancements. The ionic strength enhancements were plotted as a function of f_{ion}, Equation 22, setting $R = 4$ Å, which roughly corresponds to the size scale of a single Arg residue. The plot was not highly sensitive to the choice of R.

Stopped-flow Binding Kinetics—The kinetics of binding were characterized by rapidly mixing the SH3 domain and peptide and monitoring the progress of the reaction via intrinsic tryptophan fluorescence of the protein, which increases upon interacting with proline-rich peptides (51). We used a version of the RR peptide free of Trp and Tyr fluorophores (VSLARRPLPPLP); thus, the signal derives entirely from protein residues. We fit the binding data according to the following equation,

$$I(t) = \frac{[P](t)}{[P]_{total}} I_P + \frac{[PL](t)}{[P]_{total}} I_{PL}, \quad \text{(Eq. 12)}$$

where $I(t)$ is the fluorescence signal at time t, $[P](t)$ and $[PL](t)$ are the concentrations of free protein and bound complex at time t, $[P]_{total} = [P] + [PL]$ is the total concentration of protein, and I_P and I_{PL} are the fluorescence intensities of the free and bound states. The time dependence of $[P](t)$ is given by Ref. 52 as follows,

$$[P](t) = \frac{K_D(\alpha(1 + e^{C + \alpha k_{off} t}) - e^{C + \alpha k_{off} t} + 1)}{2(e^{C + \alpha k_{off} t} - 1)} \quad \text{(Eq. 13)}$$

where

$$\alpha = \sqrt{1 + 4[P]_{total} K_D^{-1}}, \quad \text{(Eq. 14)}$$

and

$$C = \ln\left(\frac{2[P]_0 + K_D(1 + \alpha)}{2[P]_0 + K_D(1 - \alpha)}\right), \quad \text{(Eq. 15)}$$

k_{off} is the dissociation rate constant, K_D is the equilibrium dissociation constant, and $[P]_0$ is the initial concentration of free protein at $t = 0$, which is assumed to be equal to the initial concentration of free ligand, $[L]_0 = [P]_0$. Data were analyzed by non-linear least-squares fitting with the values of $[P]_{total}$ and K_D held constant, while the values of I_P, I_{PL}, k_{off}, and $[P]_0$ were varied to minimize the function,

$$SS = \Sigma(I(t)_{calculated} - I(t)_{measured})^2 \quad \text{(Eq. 16)}$$

where $I(t)_{calculated}$ is given by Equation 1, and the sum runs over all data points. The value of $[P]_{total}$ was obtained from the absorbance of the protein sample at 280 nm (53), the concentration of the peptide was determined by amino acid analysis (54), and the value of K_D was extrapolated from temperature-dependent ITC data for the Fyn SH3/RR peptide interaction (see below). Adjusting the value of $[P]_0$ accounts for binding that occurs during the dead time of the instrument (~4 ms). The uncertainty in k_{off} was obtained by fitting random sets of the 100 individual stopped-flow traces selected according to the bootstrap method (50) and averaged. The error was taken as the S.D. value obtained after 100 iterations.

Experiments were performed using a Bio-Logic SFM 400 instrument coupled to a MOS-250 spectrometer using Biokine version 2.5 software for data acquisition. Intrinsic tryptophan fluorescence of the Fyn SH3 domain was measured with an excitation wavelength of 276 nm and a bandwidth of 20 nm. Emission at a wavelength of 320 nm and a bandwidth of 10 nm was recorded for 150 ms with measurements taken every 0.02 ms. The detector photomultiplier was operated at 860 V. For each trace, 201 μl of protein (1 μM) and 201 μl of RR peptide (1 μM) were mixed for a total injection volume of 402 μl at a flow rate of 13.5 ml s^{-1} at 5 °C.

NMR-derived Binding Kinetics—We previously characterized the binding kinetics of the RR peptide using NMR and ITC over a temperature range of 10–50 °C (33). In this prior work, we employed both CPMG and ZZ magnetization exchange NMR experiments at 20 °C, obtaining very similar values for k_{off}: 11.2 and 12.8 s^{-1}, respectively. At 10 °C, only ZZ exchange experiments were used, yielding $k_{off} = 4.5$ s^{-1}. CPMG experiments were not performed because spectral broadening is minimal at this temperature. We extrapolated the expected kinetic and thermodynamic behavior to 5 °C according to the following,

$$K_D = \exp\left(\frac{-\Delta H + T\Delta S}{RT}\right), \quad \text{(Eq. 17)}$$

$$\Delta H = \Delta H_0 + \Delta C_p(T - T_0), \quad \text{(Eq. 18)}$$

$$\Delta S = \Delta S_0 + \Delta C_p \ln\left(\frac{T}{T_0}\right), \quad \text{(Eq. 19)}$$

where $T_0 = 303.15$ K, $\Delta H_0 = 15.4$ kcal mol^{-1}, $\Delta S_0 = 20$ cal mol^{-1} K^{-1}, $\Delta C_p = 352$ cal mol^{-1} K^{-1} (33), $T = 278.15$ K, R is the universal gas constant, and the equation,

$$k_{off}(5°C) = \left(\left(\frac{278.15\ K}{283.15K}\right)\exp\left(\frac{E_a}{R}\left(\frac{1}{283.15\ K} - \frac{1}{278.15\ K}\right)\right)k_{on}(10\ °C)\right)k_D(5\ °C) \quad \text{(Eq. 20)}$$

where $k_{on}(10\ °C) = 1.03 \pm 0.05 \times 10^8$ M^{-1} s^{-1} (33), and $E_a = 3.4 \pm 0.5$ kcal mol^{-1}. This yielded $K_D(5\ °C) = 36.7$ nM and $k_{off}^{NMR}(5\ °C) = 3.3 \pm 0.2$ s^{-1}. For the sake of comparison, $K_D(10\ °C) = 46.1$ nM.

RESULTS AND DISCUSSION

NMR Titration Experiments—Series of protein ^1H-^{15}N correlation HSQC NMR spectra were collected for the Fyn SH3 domain titrated with RR, SR, and SS peptides (Fig. 1) at 40 °C. Exchange between the free and bound states was intermediate on the NMR chemical time scale (47) for the RR and SR peptides and fast for the SS peptide. The signals for many of the same protein residues were displaced by the addition of each peptide (Fig. 1, *a–c*). This suggests that all three peptides occupy the same binding site, consistent with the idea that the ΦP*X*ΦP motif is the minimal recognition sequence of the SH3 domain (37). The chemical shift displacements are color-coded on a structure of an SH3-peptide complex in Fig. 2. SS peptide titrations were repeated in the presence of 0, 0.2, and 0.3 M NaCl at 40 °C. Peak displacements (Fig. 1, *d* and *e*) were analyzed to

extract the equilibrium association constants, K_a, yielding values in good agreement with the ITC-derived measurements (Table 2). A further SS peptide titration was performed at 20 °C in the presence of 0 M NaCl. Under these conditions, exchange was on the intermediate time scale; however, peak shifts were essentially identical to those obtained at 40 °C.

Isothermal Titration Calorimetry—The affinities of the Fyn SH3 domain for the RR, SR, and SS peptides were characterized by ITC at 40 °C with NaCl concentrations ranging from 0 to 2 M (Fig. 3 and Table 2), yielding equilibrium association constants (K_a) plotted in Fig. 4. The affinity of the RR peptide shows a sharp decrease with increasing salt concentration up to about 0.25 M NaCl, followed by a gradual increase. The affinity of the SR peptide also decreases sharply up to 0.25 M NaCl. This is similar to the salt dependence of protein solubility, which typically shows an initial increase or "salting in" as electrostatic interactions are screened, followed by a decrease or "salting out" as hydrophobic interactions are enhanced by increasing salt concentration (55). The hydrophobic association of pairs of methane molecules in water and the chemical potential of methane dissolved in water both increase linearly with NaCl concentration (56, 57). The affinity of the SS peptide is roughly

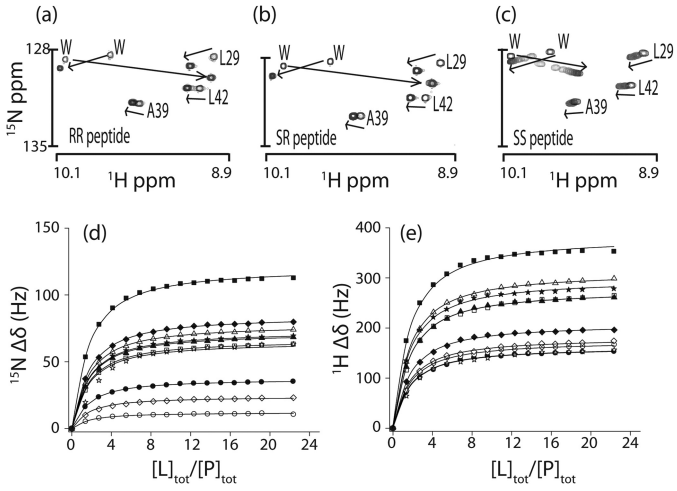

FIGURE 1. *a–c*, regions of ^{15}N/^{1}H HSQC spectra of the Fyn SH3 domain titrated with RR (*a*), SR (*b*), and SS (*c*) peptides. Shown are chemical shift displacements of SH3 domain signals in the ^{15}N (*d*) and ^{1}H (*e*) dimensions upon titration with the SS peptide. *Curves* represent the global fit to a two-state binding equation.

TABLE 2

Thermodynamic and kinetic binding parameters for the Fyn SH3 domain

[NaCl] (M)	K_A (×10^5 M^{-1})	k_{off} (s^{-1})	k_{on} (×10^8 M^{-1} s^{-1})	P_b (× 10^{-2}) (CPMG)[a]	P_b(×10^{-2}) (K_A)[b]
RR peptide					
0.0000	51.7 ± 2.7	235 ± 12.1	12.2 ± 0.9	7.3 ± 0.3	7.1
0.0080	25.6 ± 1.5				
0.0330	14.6 ± 0.3	267 ± 83.5	3.89 ± 0.01	7.4 ± 0.3	7.1
0.0500	10.3 ± 1.0				
0.1000	7.47 ± 0.2				
0.2000	5.21 ± 0.2	357 ± 13.0	1.86 ± 0.1	7.1 ± 0.2	7.2
0.3000	5.11 ± 0.2	354 ± 1.34	1.81 ± 0.1	7.3 ± 0.4	7.2
0.4000	4.50 ± 0.1				
0.5000	4.56 ± 0.2				
1.0000	5.19 ± 0.2				
1.5000	5.72 ± 0.5				
2.0000	8.68 ± 0.2				
RR peptide (15% Glycerol)					
0.0000	20.5 ± 0.5	280 ± 10 .3	5.74 ± 0.5	6.58 ± 0.3	7.1
SR peptide					
0.0000	6.31 ± 0.2	378 ± 0.3	2.39 ± 0.01	8.04 ± 0.01	7.2
0.0330	3.54 + 0.1	387 ± 0.6	1.37 ± 0.01	8.96 ± 0.1	7.2
0.2000	2.28 ± 0.23	500 ± 0.8	1.14 ± 0.1	8.21 ± 0.2	7.2
0.3000	2.33 ± 0.1	428 ± 0.6	0.99 ±0.01	7.72 ± 0.1	7.2
0.5000	2.39 ± 0.15				
1.0000	3.38± 0.1				
2.0000	6.91± 0.1				
SS peptide					
[NaCl] (M)	K_A (× 10^3 M^{-1})	k_{off} (s^{-1})	k_{on} (×10^6 M^{-1} s^{-1})		
0.0000	2.71 ± 0.2	1829 ± 127	5.09 ± 0.3		
0.2000	4.84 ± 0.1	2440 ± 239	11.8 ± 1.2		
0.3000	6.79 ± 0.1	2050 ± 239	10.9 ± 1.5		
0.5000	5.21 ± 0.1				
1.0000	9.72 ± 5.2				
2.0000	23.2 ± 4.5				
SS peptide (20°C)					
0.0000	7.87 ± 0.5	3505 ± 180	2.75 ± 0.2		
0.2000	12.10 ± 0.04	2376 ± 287	2.88 ± 0.3		
0.3000	13.13 ± 0.04	2848 ± 250	3.74 ± 0.4		

[a] Population of the bound state extracted from CPMG data.

[b] Population of the bound state calculated based on the ITC-derived affinity and concentrations of protein and peptide used.

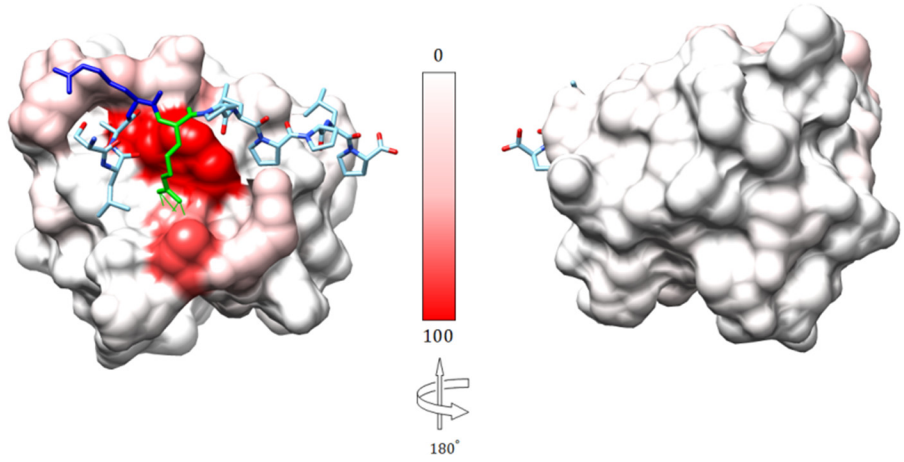

FIGURE 2. **Structure of the Fyn SH3 domain in complex with a ligand identical to the RR peptide but containing Val rather than Trp at position −8 (Protein Data Bank entry 4EIK).** Shown are relative ^{15}N/^{1}H chemical shift perturbations ($\Delta\delta^2 = (10\Delta\delta_{1H})^2 + (\Delta\delta_{15N})^2$), normalized to the largest perturbation ($\Delta\delta$ = 12.98 ppm), *color-coded* on the protein surface, from 0% (*white*) to 100% (*red*). Peptide residues Arg^{-3} (*green*) and Arg^{-4} (*blue*) are illustrated in *ball and stick* format. Hydrogen bonds between Arg^{-3} in the peptide and Asp^{17} in the Fyn SH3 domain are indicated by *green lines*.

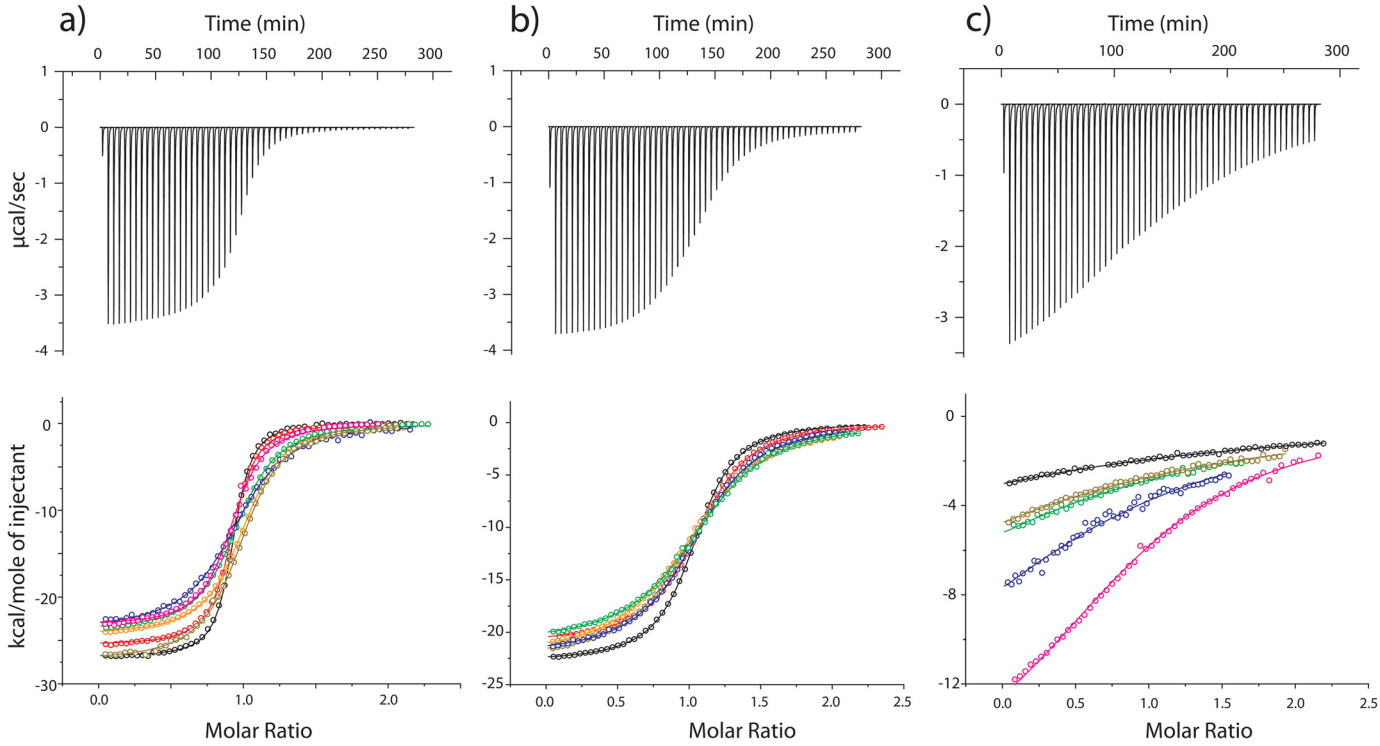

FIGURE 3. **Isothermal titration calorimetry raw thermograms (*top*) and integrated heats (*bottom*) for RR (*a*), SR (*b*), and SS (*c*) peptides binding to the Fyn SH3 domain at 40 °C and different ionic strength.** *Black*, 0 mM NaCl added; *red*, 33 mM; *orange*, 200 mM; *dark yellow*, 300 mM; *green*, 500 mM; *blue*, 1000 mM; *magenta*, 2000 mM. Raw thermograms were obtained with 0 M added salt.

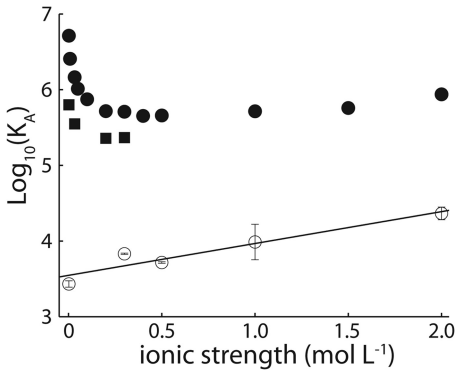

FIGURE 4. **Base 10 logarithms of affinity constants, K_a, of the Fyn SH3 domain for RR (*filled circles*), SR (*open squares*), and SS peptides (*open circles*) plotted as a function of ionic strength.** In some cases, the *error bars* are within the *symbols* used.

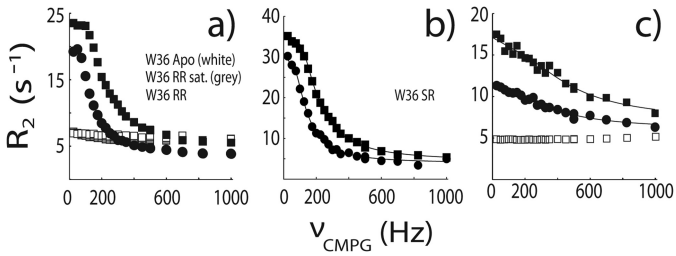

FIGURE 5. **NMR ^{15}N CPMG relaxation dispersion data for the backbone amide signal of W36 collected at 500 (*circles*) and 800 (*squares*) MHz and 0 M NaCl.** In *a*, *white*, *gray*, and *black symbols* correspond to protein samples with an RR peptide/protein ratios of 0, 300, and ~10% at 40 °C. In *b*, data were obtained with an SR peptide/protein ratio of ~10% at 40 °C. In *c*, *white* and *black symbols* correspond to SS peptide/protein ratios of 0 and ~10% at 20 °C. *Lines* indicate the global best fits as described under "Materials and Methods."

3 orders of magnitude weaker than those of the SR and RR peptides (at 0 M NaCl) and increases linearly with increasing salt concentration. This molecule is uncharged, and its binding to the SH3 domain is driven by non-polar interactions involving the ΦP*X*ΦP motif that are presumably enhanced by increasing salt concentrations. Thus, the initial downward slope of the RR affinity profile is due to the screening of electrostatics, whereas the slight upward slope at high NaCl concentrations is caused by the enhancement of hydrophobic interactions involving the ΦP*X*ΦP binding motif. As discussed below, an additional set of ITC experiments was performed for the SS peptide at 20 °C with 0, 0.2, and 0.3 M NaCl.

NMR Kinetics Experiments—The kinetics of peptide binding were characterized using NMR CPMG relaxation dispersion experiments performed on ^{15}N-enriched samples of the Fyn SH3 domain partially saturated with RR and SR peptides at 40 °C with NaCl concentrations of 0.00, 0.03, 0.20, and 0.30 M. Association/dissociation dynamics produce chemical shift fluctuations that contribute to ^{15}N transverse relaxation rates, R_2. CPMG experiments quench these contributions with variable trains of 180° refocusing radiofrequency pulses applied during a constant relaxation delay (34, 35). Plots of R_2 *versus* ν_{CPMG} are shown in Fig. 5, where $\nu_{CPMG} = 1/(2\tau)$, and τ is the delay between successive refocusing pulses. This spectral broadening reflects entirely exchange between the free and bound forms of the protein. Essentially flat dispersions are obtained for the protein in the absence of peptide, although the profiles of some residues in the free protein are very slightly sloped by 5×10^{-4} s^{-1} Hz^{-1}. This indicates that the large dispersions that we observe are not due to internal dynamics of the protein itself because these would be evident when peptide

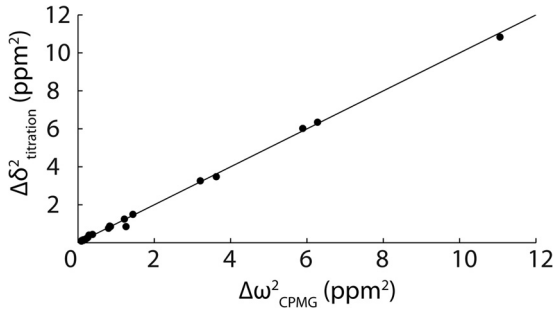

FIGURE 6. **Comparison of $\Delta\omega^2$ ^{15}N chemical shift parameters extracted from CPMG relaxation dispersion NMR experiments performed on the Fyn SH3 domain partially saturated with the RR peptide (0 M NaCl) and $\Delta\delta^2$ peak displacements from a comparison of the Fyn SH3 domain spectra free and saturated with the RR peptide (0 M NaCl).** The *line* goes through the origin with a slope of 1.

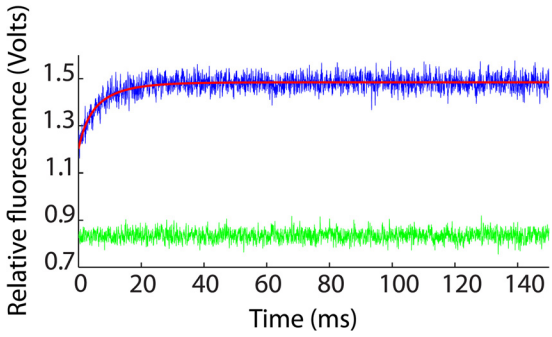

FIGURE 7. **Stopped-flow fluorescence data for the Fyn SH3 domain rapidly mixed with buffer (*green*) and with a solution of the RR peptide (*blue*).** Data shown are the averages of 100 individual stopped-flow traces. The best fit using Equation 12 is indicated with a *red line*.

is absent. Flat dispersions are also obtained with saturating amounts of the RR peptide. The populations of all protein and peptide species are at thermodynamic equilibrium throughout the CPMG experiment. Thus, any partly bound intermediate forms in the partially saturated sample would be present in the fully saturated sample as well. If the large dispersions were due to exchange between the bound state and an intermediate, they would also be observed for the fully saturated sample, which is not the case. Furthermore, chemical shift parameters extracted from the CPMG fits, $\Delta\omega^2$, provide a fingerprint of the exchanging species. In this case, we obtain quantitative agreement between $\Delta\omega^2$ and the peak displacements extracted from peptide titrations, $\Delta\delta^2$, as observed previously (33) (Fig. 6). If the large dispersions were due exchange between the free protein and a binding intermediate, such good agreement would not be expected, unless the intermediate had chemical shifts identical to those of the bound state, which is unlikely. Thus, the relaxation dispersion analysis reports on the kinetics of exchange between the free and fully bound states. Dissociation rate constants (k_{off}) were extracted from the data, as described under "Materials and Methods," and used to calculate k_{on}, according to the equation, $k_{on} = K_a \cdot k_{off}$.

Experiments with the RR peptide with 0.0 M NaCl were repeated in the presence of 15% glycerol, which translates into a 1.45-fold increase in solution viscosity, η (58). If binding rates are limited by diffusion in solution, then k_{on} should be inversely proportional to η (6), although in practice, the slope of a k_{on}/k^0_{on} *versus* η^0/η plot can diverge somewhat from the theoretical value of 1 (59). We find that the peptide binds 2.13-fold more slowly in the presence of 15% glycerol, which lies well within the range of viscosity dependences reported for diffusion-limited protein association rates (59). We also find that the association rate constant is significantly (~4-fold) more sensitive to ionic strength than the dissociation rate constant, which is a signature of diffusion-limited binding (13). In addition, we reported previously that the apparent activation enthalpy (E_a) for k_{on} is 3.4 kcal mol^{-1} (33). This matches the expected E_a = 4.5 kcal mol^{-1} for diffusion-limited reactions, reflecting the temperature dependence of water viscosity (16). Taken together, the NMR kinetics data strongly indicate that peptide binding to the SH3 domain is a diffusion-limited, two-state process.

In the case of the SS peptide at 40 °C, exchange kinetics are extremely rapid, leading to very small and essentially linear dispersion profiles. Due to their very small magnitudes, they are partially obscured by the slightly sloped profiles obtained for the free protein (which probably reflect some degree of internal motions unrelated to peptide binding). Therefore, in order to determine binding kinetics for the SS peptide, CPMG experiments were performed at 20 °C with 0, 0.2, and 0.3 M NaCl, conditions that produce large dispersions for the partially SS peptide-saturated protein sample, and completely horizontal dispersion profiles for the free protein, as shown in Fig. 5. Values of k_{off} determined at 20 °C were combined with affinities (K_a), measured by ITC at 20 °C to yield association rate constants (k_{on}). We used the previously determined value of E_a = 3.4 kcal mol^{-1} to extrapolate k_{on} for the SS peptide from 20 to 40 °C according to the equation, $k_{on}(T_2) \approx (T_2/T_1) \times k_{on}(T_1) \times \exp(E_a/R \times (1/T_1 - 1/T_2))c$ (60), where R is the gas constant. This leads to scaling of k_{on} by a factor of only 1.6, which is small compared with the up to 30-fold differences in k_{on} observed between the different peptides. Thus, the results are not sensitive to the exact choice of E_a.

Comparison of NMR and Stopped-flow Binding Kinetics—In order to cross-validate the NMR characterization of Fyn SH3 domain-peptide binding kinetics, we performed a stopped-flow spectroscopic analysis of the same system. However, the rates determined in the current study far exceed the limits of standard stopped-flow instruments (this is one of the advantages of the NMR-based approach). We therefore collected stopped-flow data at 5 °C, in order to slow the kinetics sufficiently for them to be amenable to this type of analysis. Fluorescence traces for the SH3 domain injected with buffer (*green*) and a peptide solution (*blue*) are shown in Fig. 7, with $t = 0$ aligned to the end of the injection. As expected, the fluorescence signal for the protein-peptide pair shows a time-dependent increase after the injection due to evolution of the binding reaction. This signal is above that of the free protein at $t = 0$ due to binding that occurs during the dead time of the instrument, which is about 4 ms. Analysis of the stopped-flow data yields $k^{SF}_{off}(5\ °C) = 8.9 \pm 0.6\ s^{-1}$, whereas the NMR kinetics method yields $k^{NMR}_{off}(5\ °C) = 3.3 \pm 0.2\ s^{-1}$, as described under "Materials and Methods." These two values differ by about a factor of 3, which we believe is excellent agreement for such different experimental modalities. This gives us further confidence in the NMR-based kinetics method.

Electrostatic Enhancement of Association Rates—We investigated the influence of electrostatics on SH3 domain ligand binding kinetics by varying the ionic strength of the samples, in order to attenuate long range coulombic interactions, and by comparing results for the RR, SR, and SS peptides, which carry formal charges of +2, +1, and 0. The screening of coulombic interactions by electrolyte solutions was analyzed in terms of the electrostatic attraction of two oppositely charged spheres with radii r, a center-center separation of $2r$, and charges $\pm Z$. Relative to infinite separation, the potential energy, V, is given by the expression (61, 62),

$$V = -\frac{Z^2e^2}{2r\epsilon} \times f_{ion}, \quad \text{(Eq. 21)}$$

$$f_{ion} = \frac{\exp(-\kappa r)}{1 + \kappa r}, \quad \text{(Eq. 22)}$$

where e is the elemental charge, ϵ is the dielectric constant of the medium, κ is the inverse Debye length,

$$\kappa = \sqrt{\frac{4\pi e^2}{k_B T}}\sqrt{I}, \quad \text{(Eq. 23)}$$

k_B is the Boltzmann constant, and I is the ionic strength. The parameter f_{ion} describes the ionic strength dependence of the potential energy, with limiting values of 1 (full interaction strength) in the absence of salt, and 0 (zero interaction strength) at infinite salt concentration.

The logarithms of k_{on} are plotted as a function of f_{ion} for the RR, SR, and SS peptides in Fig. 8*a*, together with linear regression lines. Data for the RR and SR peptides have positive slopes, as expected, because larger values of f_{ion} correspond to lower salt concentrations, greater electrostatic stabilization of the transition state, and faster association. The data for the SS peptide are close to horizontal, as expected for an uncharged ligand. The slightly negative slope may be due to weak hydrophobic stabilization of the transition state that is enhanced at high salt concentrations. Notably, the lines for the three peptides nearly intersect at $f_{ion} = 0$ and a k_{on} value of about 6×10^7 M^{-1} s^{-1}. This corresponds to the basal, or electrostatic-free, association rate. The close agreement of basal association rates obtained for the three different peptides gives us confidence in the reliability of the extrapolation along f_{ion}. The slopes of the lines correspond to the logarithms of the maximum electrostatic enhancement of binding with zero ionic strength, $\log(k_{on}^{enhanced}/k_{on}^{basal})$. We find that long range coulombic interactions accelerate binding of the RR and SR peptides by 23.1- and 4.42-fold, respectively, as listed in Table 1.

The basal association rate for the SH3 domain is significantly greater, and the extent of electrostatic enhancement is much less, than observed previously for long lived complexes. Association rates for a data set of five different systems (13) are plotted as a function of f_{ion} in Fig. 6*b*, and the basal association rates and electrostatic enhancements extracted from the linear fits are listed in Table 1. These proteins bind roughly 10^3 to 10^{10}-fold more tightly and dissociate 10^3 to 10^9-fold more slowly than the SH3 domain studied here. Notably, all of these basal, electrostatic association rates are 10–100-fold slower than those obtained for the SH3 domain, whereas the electrostatic rate enhancements are 10^2 to 10^4-fold greater.

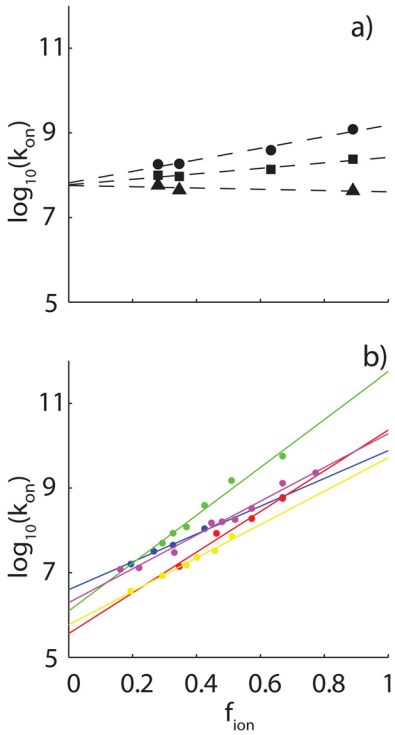

FIGURE 8. **Ionic strength dependence of association rates.** *a*, NMR and ITC-derived association rate constants (k_{on}) for the RR (*circles*) and SR (*squares*) and SS (*triangles*) peptides binding to the Fyn SH3 domain, plotted as a function of f_{ion} (Equation 22), which takes values between 1 at zero ionic strength and 0 at infinite ionic strength. *Dashed lines*, linear regression fits of the data. *b*, association constants for barnase-barstar (*blue*), shaker K^+ channel-peptide toxin Lq2 (*red*), E9 DNase-immunity protein Im9 (*green*), heterodimeric leucine zipper (*yellow*), and acetylcholinesterase-fasciculin 2 (*magenta*) plotted as a function of f_{ion}.

It is likely that these differences are due to differences in the nature of the binding surfaces for the SH3 domain compared with the proteins in the long lived complex database. The barnase-barstar interface is fairly typical of those in the database in terms of size and complexity. It buries 1590 Å^2 of accessible surface area and involves the formation of 14 specific hydrogen bonds (63). In this case, only about 1 molecular collision in 1700 aligns the binding surfaces sufficiently accurately to proceed to the fully bound state in the absence of electrostatic enhancement, assuming no charged interactions and a molecular collision frequency of 6.6×10^9 M^{-1} s^{-1} (12). In contrast, the complex formed by the SH3 domain and ΦP*X*ΦP motif buries only 600 Å^2 and is stabilized entirely by hydrophobic interactions (40). In this case, about 1 in every 160 SH3-peptide collisions is sufficiently well aligned to progress to the bound state. Docking of the SS peptide onto the SH3 binding surface involves a significantly smaller contact area with fewer specific pairwise interactions. This probably results in less stringent geometric requirements for molecular collisions to lead to successful docking of the SS peptide and a more rapid basal association rate.

A less geometrically restricted transition state could explain our observation of lower electrostatic enhancement of SH3-peptide association rates compared with that of barnase-barstar and other long lived complexes. For barnase-barstar, it

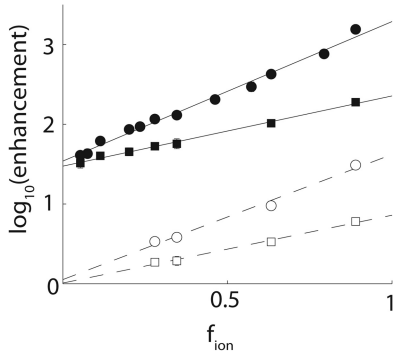

FIGURE 9. **Enhancements in affinities ($K_a^{SR,RR}/K_a^{SS}$; *solid lines*, *filled symbols*) and association rates ($k_{on}^{SR,RR}/k_{on}^{SS}$; *dashed lines*, *open symbols*) for the RR (*circles*) and SR (*squares*) peptides relative to the SS peptide, plotted as a function of f_{ion}.**

was found that the transition state is stabilized by specific charged residues that are in close proximity in the stereospecific complex. This implies that these residues are correctly oriented with respect to one another at the rate-limiting step of binding (5). The SH3 domain exhibits a greater basal association rate, suggesting that the transition state is less geometrically constrained. Thus, fewer specific interactions may be formed between charged residues in this state, leading to a smaller degree of electrostatic stabilization.

Thus, the SH3 domain and target peptide do not rely as heavily upon electrostatic enhancement to achieve rapid association kinetics as do many previously studied long lived complexes. It has been noted previously that the interfaces of high-affinity complexes tend to contain more charged residues than those of low-affinity ones, and that these coulombic interactions are sometimes, but not always, thermodynamically stabilizing (64). This is consistent with higher affinity complexes relying more heavily on electrostatic enhancement to achieve rapid binding kinetics than weaker complexes; however, the question is far from resolved.

Arginine Interactions in the Transition State and Bound State—In order to clarify the role played by the peptide arginine residues in the SH3 domain binding pathway, we compared K_a and k_{on} values for the RR and SR peptides with those of the SS peptide. The SS peptide carries no formal charges and binds in the same location as the SR and RR peptides, as evinced by similar patterns of peak movements in protein NMR titration experiments. The ratios of K_a and k_{on} obtained for the RR and SR peptides relative to those of the SS peptide describe the contributions of the conserved (Arg^{-3}) and "extra" (Arg^{-4}) Arg residues to the stabilities of the fully bound and transition states. The logarithms of the RR/SS and SR/SS ratios are plotted as a function of f_{ion} in Fig. 9 and exhibit excellent linear correlations over their full ranges of roughly 2 orders of magnitude. When extrapolated to infinite salt concentration at the *y* intercept, the affinity of the SR peptide is still enhanced by a factor of 26, relative to the SS peptide, which translates into a stabilization of the bound state by 2.0 kcal mol^{-1}. This enhancement is due to interactions formed by Arg^{-3} that are not screened by salt and therefore almost certainly involve short range forces. The slope for the RR peptide is greater than that of the SR peptide by about a factor of 2 in Fig. 9, consistent with the 2-fold difference in formal charge. However, when extrapolated to infinite salt concentration, the affinities of the two peptides are virtually identical, as evinced by the intersection of the two lines at the *y* axis (Fig. 7, *solid lines*). Thus, the "extra" Arg^{-4} forms long range electrostatic interactions in the bound state but no energetically significant short range (*i.e.* unscreened) interactions.

This is consistent with the x-ray crystal structure of the Fyn SH3 domain bound to a ligand very similar to the RR peptide used in this study ($Trp^{-8} \rightarrow Val^{-8}$), shown in Fig. 2 (40). The conserved Arg^{-3} forms a salt bridge (*i.e.* hydrogen-bonds) with Asp^{17}, whereas the aliphatic portion of the residue packs against Trp^{36}. In contrast, the "extra" Arg, Arg^{-4}, points away from Asp^{17} and makes no additional hydrogen bonds. However, negatively charged Glu^{33} and Glu^{34} are within about 6.5 Å, well positioned to interact with Arg^{-4} electrostatically. Guanidinium ions, equivalent to the guanidino moiety of the Arg side chain, interact with the Fyn SH3 domain specifically at the peptide binding site and compete with the RR peptide (65). Together, these data strongly suggest that the guanidino moiety of Arg^{-3} interacts with Fyn SH3 domain via a network of hydrogen bonds, whereas Arg^{-4} forms looser, long range electrostatic interactions in the fully bound complex.

The pattern of enhancements seen for k_{on} is similar but differs in an important respect. At 0 M NaCl, the RR peptide binds 5-fold more rapidly than the SR peptide, which binds 6-fold more rapidly than the SS peptide. This is consistent with both Arg^{-3} and Arg^{-4} forming long range electrostatic interactions in the transition state. However, in the extrapolation to infinite salt concentration, both RR and SR peptides bind with rates that are nearly identical to the value determined for the SS peptide. All of the interactions formed by the peptide Arg residues in the transition state are thus electrostatic and long range (*i.e.* are screened by salt). The short range interactions involving Arg^{-3} that are present in the fully bound complex are only formed after the protein-peptide pair have passed through the high-energy transition state (*i.e.* near the end of the binding process). The transition states of far more tightly binding partners are believed to be similarly dominated by long range electrostatic interactions and lacking in short range contacts (5, 14, 15, 22).

Ionic Strength Dependence of Dissociation Rates—For diffusion-limited binding reactions, values of k_{on} are typically far more sensitive to ionic strength than are values of k_{off} (1, 10, 26). In the case of the RR peptide, k_{on} is about 4 times more sensitive to ionic strength than k_{off}. This has been explained in terms of the structure of the transition state (13). Long range electrostatic interactions are fairly insensitive to small changes in charge separation. Thus, if the two binding partners remain close in the transition state, then long range electrostatics contribute similarly to the stabilities of the fully bound and transition states. Increasing the ionic strength screens the long range charge interactions present in both states to equal extents. Thus, the barrier to dissociation is not greatly affected, and k_{off} is essentially unchanged. In contrast, destabilization of the transition state by added salt increases the barrier to association and slows binding rates.

However, this explanation appears inconsistent with mutational analyses of charge interactions in the fully bound and transition states. In the case of barnase-barstar, mutagenesis-derived coupling energies between charged residues in the fully bound state range from 1 to 7 kcal mol^{-1} (40), whereas coupling energies in the transition state are less than 0.5 kcal mol^{-1} (5). Similarly, the SS peptide binds 250-fold more weakly than the SR peptide but only 6-fold more slowly. The SS peptide binds 1900-fold more weakly and only 29-fold more slowly than the RR peptide in the absence of salt. These results indicate that the interactions of charged residues are much weaker in the transition state than in the fully bound state. Adding salt should significantly destabilize the bound state without significantly affecting the transition state and thus should increase dissociation rates. Our results provide a simple explanation for this apparent contradiction. We directly measured electrostatic-free basal affinities and association rates for the SS peptide, which allowed us to separate the interaction energies of Arg^{-3} and Arg^{-4} into long range "screenable" electrostatic and short range "unscreenable" components. Notably, the long range components are comparable for the fully bound and transition states. For the SR compared with the SS peptide, long range interactions enhance the affinity and association rate by factors of 9 and 6, respectively, at 0 M NaCl, compared with 250- and 6-fold total enhancements. For the RR peptide, these long range enhancement factors are 73 and 29, compared with 1900- and 29-fold total enhancements. Thus, for the Fyn SH3 domain, long range electrostatic interactions are similar in the fully bound and transition states, leading to k_{off} values that are relatively insensitive to ionic strength. This has the implication that the peptide and SH3 domain are separated by a relatively short distance in the transition state, as seen previously for long lived protein complexes (13).

Conclusions—Most of our knowledge of protein binding kinetics derives from studies of extremely stable long lived complexes. The binding kinetics of short lived protein complexes are less well understood because these systems are challenging to characterize experimentally. We have applied a recently developed combination of NMR and ITC to study complexes of the Fyn SH3 domain and several peptides whose bound lifetimes are as short as 0.3 ms. This is beyond the range of standard stopped-flow techniques used to measure binding kinetics. We find that although the binding pathways of these transient SH3 complexes are similar to those of high-affinity long lived complexes, they differ in some important respects.

For the SH3 domain, as well as for high-affinity binding partners, the transition state is stabilized by long range electrostatic interactions, whereas short range stereo-specific contacts are formed late in the binding pathway. We find that the contributions of long range electrostatic interactions to both the fully bound and transition states are quite similar, implying that the separation between the SH3 domain and peptide is not large in the transition state. A similar situation is believed to hold true for the transition states of high-affinity systems. Thus, structural compactness and the dominance of long range electrostatic interactions appear to be universal features of diffusion-limited binding pathways involving affinities and lifetimes spanning up to 7 orders of magnitude.

However, the electrostatic acceleration of SH3 domain association rates is several orders of magnitude less than has been previously observed for stable long lived protein complexes. In contrast, the electrostatic-free basal association rate is much greater, possibly because of looser geometrical restrictions for molecular collisions to proceed to the bound state. This raises the interesting question of whether or not this is a general phenomenon. Do weakly bound, transient complexes intrinsically have more rapid basal association rates and less reliance on electrostatic enhancement than do tightly bound, long lived complexes? If so, how does this relate to the compositions and geometries of the binding interfaces? The combined NMR and calorimetric approach used here is uniquely suited for studying transient complexes to gain a better understanding of the relationships among binding affinities, basal association kinetics, and electrostatic rate enhancements and to shed light on the fundamental principles of molecular recognition.

Acknowledgment—NMR experiments were recorded at the Québec/Eastern Canada High Field NMR Facility, supported by McGill University and Groupe de Recherche Axé sur la Structure des Protéines (GRASP).

REFERENCES

1. Radić, Z., Kirchhoff, P. D., Quinn, D. M., McCammon, J. A., and Taylor, P. (1997) Electrostatic influence on the kinetics of ligand binding to acetylcholinesterase. Distinctions between active center ligands and fasciculin. *J. Biol. Chem.* **272,** 23265–23277
2. Foote, J., and Milstein, C. (1991) Kinetic maturation of an immune response. *Nature* **352,** 530–532
3. Wang, Y., Shen, B. J., and Sebald, W. (1997) A mixed-charge pair in human interleukin 4 dominates high-affinity interaction with the receptor α chain. *Proc. Natl. Acad. Sci. U.S.A.* **94,** 1657–1662
4. Jucovic, M., and Hartley, R. W. (1996) Protein-protein interaction: a genetic selection for compensating mutations at the barnase-barstar interface. *Proc. Natl. Acad. Sci. U.S.A.* **93,** 2343–2347
5. Schreiber, G., and Fersht, A. R. (1996) Rapid, electrostatically assisted association of proteins. *Nat. Struct. Biol.* **3,** 427–431
6. Berg, O. G., and von Hippel, P. H. (1985) Diffusion-controlled macromolecular interactions. *Annu. Rev. Biophys. Biophys. Chem.* **14,** 131–160
7. Zhou, H. X. (1997) Enhancement of protein-protein association rate by interaction potential: accuracy of prediction based on local Boltzmann factor. *Biophys. J.* **73,** 2441–2445
8. Northrup, S. H., and Erickson, H. P. (1992) Kinetics of protein-protein association explained by Brownian dynamics computer simulation. *Proc. Natl. Acad. Sci. U.S.A.* **89,** 3338–3342
9. Gabdoulline, R. R., and Wade, R. C. (2002) Biomolecular diffusional association. *Curr. Opin. Struct. Biol.* **12,** 204–213
10. Wallis, R., Moore, G. R., James, R., and Kleanthous, C. (1995) Protein-Protein Interactions in Colicin E9 Dnase-Immunity Protein Complexes. 1. Diffusion-Controlled Association and Femtomolar Binding for the Cognate Complex. *Biochemistry* **34,** 13743–13750
11. Shen, B. J., Hage, T., and Sebald, W. (1996) Global and local determinants for the kinetics of interleukin-4/interleukin-4 receptor α chain interaction: a biosensor study employing recombinant interleukin-4-binding protein. *Eur. J. Biochem.* **240,** 252–261
12. Janin, J. (1997) The kinetics of protein-protein recognition. *Proteins Struct. Funct. Genet.* **28,** 153–161
13. Zhou, H. X. (2001) Disparate ionic-strength dependencies of on and off rates in protein-protein association. *Biopolymers* **59,** 427–433
14. Alsallaq, R., and Zhou, H. X. (2008) Electrostatic rate enhancement and transient complex of protein-protein association. *Proteins* **71,** 320–335
15. Alsallaq, R., and Zhou, H.-X. (2007) Prediction of protein-protein associ-

ation rates from a transition-state theory. *Structure* **15,** 215–224
16. Pilling, M., and Seakins, P. (1995) *Reaction Kinetics*, Chapter 6, p. 146, Oxford University Press, Oxford
17. Szabo, A., Shoup, D., Northrup, S., and McCammon, J. A. (1982) Stochastically gated diffusion-influenced reactions. *J. Chem. Phys.* **77,** 4484–4493
18. Sommer, J., Jonah, C., Fukuda, R., and Bersohn, R. (1982) Production and subsequent 2nd-order decomposition of protein disulfide anions: lengthy collisions between proteins. *J. Mol. Biol.* **159,** 721–744
19. Camacho, C. J., Kimura, S. R., DeLisi, C., and Vajda, S. (2000) Kinetics of desolvation-mediated protein-protein binding. *Biophys. J.* **78,** 1094–1105
20. Camacho, C. J., Weng, Z., Vajda, S., and DeLisi, C. (1999) Free energy landscapes of encounter complexes in protein-protein association. *Biophys. J.* **76,** 1166–1178
21. Northrup, S. H., Thomasson, K. A., Miller, C. M., Barker, P. D., Eltis, L. D., Guillemette, J. G., Inglis, S. C., and Mauk, A. G. (1993) Effects of charged amino acid mutations on the bimolecular kinetics of reduction of yeast iso-1-ferricytochrome *c* by bovine ferrocytochrome b_5. *Biochemistry* **32,** 6613–6623
22. Vijayakumar, M., Wong, K. Y., Schreiber, G., Fersht, A. R., Szabo, A., and Zhou, H. X. (1998) Electrostatic enhancement of diffusion-controlled protein-protein association: comparison of theory and experiment on barnase and barstar. *J. Mol. Biol.* **278,** 1015–1024
23. Volkov, A. N., Ubbink, M., and van Nuland, N. A. J. (2010) Mapping the encounter state of a transient protein complex by PRE NMR spectroscopy. *J. Biomol. NMR* **48,** 225–236
24. Tang, C., Iwahara, J., and Clore, G. M. (2006) Visualization of transient encounter complexes in protein-protein association. *Nature* **444,** 383–386
25. Sugase, K., Dyson, H. J., and Wright, P. E. (2007) Mechanism of coupled folding and binding of an intrinsically disordered protein. *Nature* **447,** 1021–1025
26. Schreiber, G., and Fersht, A. R. (1993) Interaction of barnase with its polypeptide inhibitor barstar studied by protein engineering. *Biochemistry* **32,** 5145–5150
27. Sydor, J. R., Engelhard, M., Wittinghofer, A., Goody, R. S., and Herrmann, C. (1998) Transient kinetic studies on the interaction of ras and the Ras-binding domain of c-Raf-1 reveal rapid equilibration of the complex. *Biochemistry* **37,** 14292–14299
28. Stone, S. R., Dennis, S., and Hofsteenge, J. (1989) Quantitative evaluation of the contribution of ionic interactions to the formation of the thrombin-hirudin complex. *Biochemistry* **28,** 6857–6863
29. Taylor, M. G., Rajpal, A., and Kirsch, J. F. (1998) Kinetic epitope mapping of the chicken lysozyme·HyHEL-10 Fab complex: delineation of docking trajectories. *Protein Sci.* **7,** 1857–1867
30. Altschuh, D., Dubs, M. C., Weiss, E., Zeder-Lutz, G., and Van Regenmortel, M. H. (1992) Determination of kinetic constants for the interaction between a monoclonal antibody and peptides using surface plasmon resonance. *Biochemistry* **31,** 6298–6304
31. England, P., Brégégère, F., and Bedouelle, H. (1997) Energetic and kinetic contributions of contact residues of antibody D1.3 in the interaction with lysozyme. *Biochemistry* **36,** 164–172
32. Vallurupalli, P., Hansen, D. F., Stollar, E., Meirovitch, E., and Kay, L. E. (2007) Measurement of bond vector orientations in invisible excited states of proteins. *Proc. Natl. Acad. Sci. U.S.A.* **104,** 18473–18477
33. Demers, J. P., and Mittermaier, A. (2009) Binding mechanism of an SH3 domain studied by NMR and ITC. *J. Am. Chem. Soc.* **131,** 4355–4367
34. Mittermaier, A. K., and Kay, L. E. (2009) Observing biological dynamics at atomic resolution using NMR. *Trends Biochem. Sci.* **34,** 601–611
35. Palmer, A. G., 3rd, Kroenke, C. D., and Loria, J. P. (2001) NMR methods for quantifying microsecond-to-millisecond motions in biological macromolecules. *Methods Enzymol.* **339,** 204–238
36. Hansen, D. F., Vallurupalli, P., and Kay, L. E. (2008) An improved ^{15}N relaxation dispersion experiment for the measurement of millisecond time-scale dynamics in proteins. *J. Phys. Chem. B* **112,** 5898–5904
37. Yu, H., Chen, J. K., Feng, S., Dalgarno, D. C., Brauer, A. W., and Schreiber, S. L. (1994) Structural basis for the binding of proline-rich peptides to SH3 domains. *Cell* **76,** 933–945
38. Mayer, B. J. (2001) SH3 domains: complexity in moderation. *J. Cell Sci.* **114,** 1253–1263
39. Hansen, D. F., Vallurupalli, P., Lundström, P., Neudecker, P., and Kay, L. E. (2008) Probing chemical shifts of invisible states of proteins with relaxation dispersion NMR spectroscopy: how well can we do? *J. Am. Chem. Soc.* **130,** 2667–2675
40. Feng, S. B., Kasahara, C., Rickles, R. J., and Schreiber, S. L. (1995) Specific interactions outside the proline-rich core of two classes of Src homology 3 ligands. *Proc. Natl. Acad. Sci. U.S.A.* **92,** 12408–12415
41. Mittermaier, A., and Kay, L. E. (2004) The response of internal dynamics to hydrophobic core mutations in the SH3 domain from the Fyn tyrosine kinase. *Protein Sci.* **13,** 1088–1099
42. Bolzani, R., Ruggeri, F., and Olivo, O. M. (1979) Average normal temperature of the chicken in the morning and after 1–2 days of fasting. *Boll. Soc. Ital. Biol. Sper.* **55,** 1618–1622
43. Wishart, D. S., Bigam, C. G., Yao, J., Abildgaard, F., Dyson, H. J., Oldfield, E., Markley, J. L., and Sykes, B. D. (1995) ^{1}H, ^{13}C and ^{15}N chemical shift referencing in biomolecular NMR. *J. Biomol. NMR* **6,** 135–140
44. Macomber, R. S. (1992) An introduction to NMR titration for studying rapid reversible complexation. *J. Chem. Ed.* **69,** 375–378
45. Luz, Z., and Meiboom, S. (1963) Nuclear magnetic resonance study of the protolysis of trimethylammonium ion in aqueous solution: order of the reaction with respect to solvent. *J. Chem. Phys.* **39,** 366
46. Carver, J. P., and Richards, R. E. (1972) A general two-site solution for the chemical exchange produced dependence of T2 upon the Carr-Purcell pulse separation. *J. Magn. Reson.* **6,** 89–105
47. Millet, O., Loria, J. P., Kroenke, C. D., Pons, M., and Palmer, A. G. (2000) The static magnetic field dependence of chemical exchange linebroadening defines the NMR chemical shift time scale. *J. Am. Chem. Soc.* **122,** 2867–2877
48. Ishima, R., and Torchia, D. (2005) Error estimation and global fitting in transverse-relaxation dispersion experiments to determine chemical-exchange parameters. *J. Biomol. NMR* **32,** 41–54
49. Mulder, F. A. A., Mittermaier, A., Hon, B., Dahlquist, F. W., and Kay, L. E. (2001) Studying excited states of proteins by NMR spectroscopy. *Nat. Struct. Biol.* **8,** 932–935
50. Efron, B., and Tibshirani, R. (1986) Bootstrap methods for standard errors, confidence intervals and other measures of statistical accuracy. *Stat. Sci.* **1,** 54–75
51. Di Nardo, A. A., Larson, S. M., and Davidson, A. R. (2003) The relationship between conservation, thermodynamic stability, and function in the SH3 domain hydrophobic core. *J. Mol. Biol.* **333,** 641–655
52. Cantor, C., and Schimmel, P. (1980) *Biophysical Chemistry Part III: The Behaviour of Biological Macromolecules*, Chapter 16, p. 892, W.H. Freeman and Co., New York
53. Pace, C. N., Vajdos, F., Fee, L., Grimsley, G., and Gray, T. (1995) How to measure and predict the molar absorption coefficient of a protein. *Protein Sci.* **4,** 2411–2423
54. Smith, A. J. (1997) Amino Acid Analysis. *Methods Enzymol.* **289,** 419–426
55. Melander, W., and Horváth, C. (1977) Salt effects on hydrophobic interactions in precipitation and chromatography of proteins: interpretation of lyotropic series. *Arch. Biochem. Biophys.* **183,** 200–215
56. Bennaim, A., and Yaacobi, M. (1974) Effects of solutes on strength of hydrophobic interaction and its temperature-dependence. *J. Phys. Chem.* **78,** 170–175
57. Docherty, H., Galindo, A., Sanz, E., and Vega, C. (2007) Investigation of the salting out of methane from aqueous electrolyte solutions using computer simulations. *J. Phys. Chem. B* **111,** 8993–9000
58. Segur, J. B., and Oberstar, H. E. (1951) Viscosity of glycerol and its aqueous solutions. *Ind. Eng. Chem.* **43,** 2117–2120
59. Schreiber, G. (2002) Kinetic studies of protein-protein interactions. *Curr. Opin. Struct. Biol.* **12,** 41–47
60. Eyring, H. (1935) The Activated Complex in Chemical Reactions. *J. Chem. Phys.* **3,** 107–115
61. Wherland, S., and Gray, H. B. (1976) Metalloprotein electron-transfer reactions: analysis of reactivity of horse heart cytochrome-C with inorganic complexes. *Proc. Natl. Acad. Sci. U.S.A.* **73,** 2950–2954
62. Alberty, R. A., and Hammes, G. G. (1958) Application of the theory of diffusion-controlled reactions to enzyme kinetics. *J. Phys. Chem* **62,**

154–159
63. Buckle, A. M., Schreiber, G., and Fersht, A. R. (1994) Protein-protein recognition: crystal structural-analysis of a barnase barstar complex at 2.0-angstrom resolution. *Biochemistry* **33,** 8878–8889
64. Xu, D., Lin, S. L., and Nussinov, R. (1997) Protein binding versus protein folding: the role of hydrophilic bridges in protein associations. *J. Mol. Biol.* **265,** 68–84
65. Zarrine-Afsar, A., Mittermaier, A., Kay, L. E., and Davidson, A. R. (2006) Protein stabilization by specific binding of guanidinium to a functional arginine-binding surface on an SH3 domain. *Protein Sci.* **15,** 162–170
66. Escobar, L., Root, M. J., and MacKinnon, R. (1993) Influence of protein surface charge on the bimolecular kinetics of a potassium channel peptide inhibitor. *Biochemistry* **32,** 6982–6987
67. Wallis, R., Leung, K. Y., Pommer, A. J., Videler, H., Moore, G. R., James, R., and Kleanthous, C. (1995) Protein-protein interactions in colicin E9 DNase-immunity protein complexes. 2. Cognate and noncognate interactions that span the millimolar to femtomolar affinity range. *Biochemistry* **34,** 13751–13759
68. Wendt, H., Leder, L., Härmä, H., Jelesarov, I., Baici, A., and Bosshard, H. R. (1997) Very rapid, ionic strength-dependent association and folding of a heterodimeric leucine zipper. *Biochemistry* **36,** 204–213